Environmental Science & Technology

pubs.acs.org/est

Article

Marine Colloids Boost Nitrogen Fixation in *Trichodesmium erythraeum* by Photoelectrophy

Weilu Kang, Li Mu, and Xiangang Hu*

Cite This: *Environ. Sci. Technol.* 2024, 58, 9236−9249

Read Online

ACCESS | Metrics & More | Article Recommendations | Supporting Information

ABSTRACT: Nitrogen fixation by the diazotrophic cyanobacterium *Trichodesmium* contributes up to 50% of the bioavailable nitrogen in the ocean. N_2 fixation by *Trichodesmium* is limited by the availability of nutrients, such as iron (Fe) and phosphorus (P). Although colloids are ubiquitous in the ocean, the effects of Fe limitation on nitrogen fixation by marine colloids (MC) and the related mechanisms are largely unexplored. In this study, we found that MC exhibit photoelectrochemical properties that boost nitrogen fixation by photoelectrophy in *Trichodesmium erythraeum*. MC efficiently promote photosynthesis in *T. erythraeum*, thus enhancing its growth. Photoexcited electrons from MC are directly transferred to the photosynthetic electron transport chain and contribute to nitrogen fixation and ammonia assimilation. Transcriptomic analysis revealed that MC significantly upregulates genes related to the electron transport chain, photosystem, and photosynthesis, which is consistent with elevated photosynthetic capacities (e.g., F_v/F_m and carboxysomes). As a result, MC increase the N_2 fixation rate by 67.5−89.3%. Our findings highlight a proof-of-concept electron transfer pathway by which MC boost nitrogen fixation, broadening our knowledge on the role of ubiquitous colloids in marine nitrogen biogeochemistry.

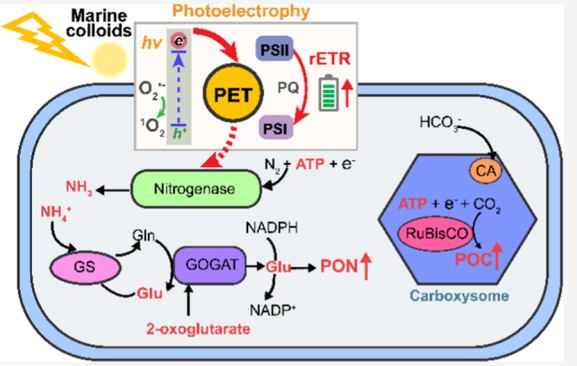

KEYWORDS: *photoelectrophy, marine colloids, cyanobacteria, electron transfer, nitrogen fixation*

INTRODUCTION

Nitrogen fixation by cyanobacteria is an important route through which bioavailable nitrogen is supplied to the ocean, contributing to the biogeochemical cycling of marine nitrogen and carbon.[1−3] Primary production is limited by nitrogen in low-nutrient open ocean ecosystems (~75% of the ocean's surface area).[2] Diazotrophs are the primary nitrogen contributors that supply bioavailable forms of nitrogen (e.g., ammonia and amino acids) in oligotrophic oceans.[4] The marine cyanobacterium *Trichodesmium* performs nitrogen fixation and photosynthesis simultaneously during the photoperiod, providing approximately 80 Tg of fixed nitrogen to the ocean surface each year.[5] *Trichodesmium* fixes up to half of the new nitrogen used for primary production,[6,7] and its nitrogen fixation is controlled by temperature, light, phosphorus, iron (Fe) availability, and other unknown environmental factors in the global ocean.[8]

Fe is an important limiting factor for N_2 fixation and controls the large-scale distribution and activity of diazotrophs due to the comparatively high cellular Fe supply required for nitrogenase and photosynthetic electron transport (PET).[9−12] Nitrogenase, the only enzyme that can convert N_2 to NH_3, consists of a reducing and a catalytic subunit, i.e., the homodimeric Fe protein and the heterotetrameric MoFe protein.[13,14] The supply of Fe to oligotrophic surface waters in the ocean is expected to decrease in the future as a result of global warming.[15] Marine colloids (MC) are widely distributed in the ocean and are defined as particles with a size fraction between 1 and 1000 nm and at least one dimension less than 100 nm.[16,17] MC constitute a large portion (30−60%) of the bulk dissolved organic matter (DOM) pool in aquatic environments.[18,19] In addition to having high specific surface areas and complexation capacities, MC exhibit redox activity by triggering electron transfer through hydroquinone/quinone and other redox-active molecules.[20,21] DOM is an active photosensitizer that generates reactive photoinduced species, such as singlet oxygen ($^1O_2$), hydroxyl radicals ($^•OH$), and hydrated electrons, upon illumination.[22] Recent evidence has demonstrated that phototrophs can directly use solid-phase conductive substances for electron transfer to carry out carbon and nitrogen fixation.[23,24] For example, the photoheterotrophic bacterium *Rhodopseudomonas palustris* can utilize photoexcited electrons from cadmium sulfide (CdS) nanoparticles (NPs) to

Received: February 21, 2024
Revised: May 2, 2024
Accepted: May 3, 2024
Published: May 15, 2024

https://doi.org/10.1021/acs.est.4c01849
Environ. Sci. Technol. 2024, 58, 9236−9249

increase N_2 fixation and solid biomass production.[25] These studies highlight the opportunity for the photoelectrophic effect to promote nitrogen fixation in the ocean.

In this study, we identified a new pathway, by which photoinduced electrons from MC promoted biological nitrogen fixation in *Trichodesmium erythraeum*. Bioelectrochemistry, electron spin resonance (ESR), nanoscale secondary ion mass spectrometry (NanoSIMS) imaging, and electron transport inhibition experiments showed that photoexcited electrons from MC integrate the electron transfer process in photosynthesis and contribute to light-driven nitrogen assimilation. This work highlights the electron transfer pathway driven by MC at biotic−abiotic interfaces that boost carbon and nitrogen fixation, providing a novel mechanism for biological modulation and sustainability in cyanobacteria.

MATERIALS AND METHODS

Isolation and Characterization of Marine Colloids. Surface seawater was collected from the Bohai Sea (39°00.09′N, 117°53.97′E) in October 2022 and immediately transported to the laboratory for MC isolation. MC (1−100 nm, also called nanocolloids) were extracted using prefiltration, cross-flow ultrafiltration, and dialysis, as previously described.[26] Briefly, 2 L of surface water was filtered through a 0.1 μm Millipore poly(ether sulfone) (PES) membrane. Then, the prefiltered water was injected into a cross-flow ultrafiltration system (Figure S1), which included a 5000 Da molecular weight cutoff PES module (VF20P1, Sartorius, Germany) and a peristaltic pump (YZ2515x, Longer Precision Pump Co., Ltd., China), and 30 mL of the concentrated sample was reserved. Subsequently, the concentrated samples were dialyzed using 5 kDa dialysis membranes (B0052, Viskase) and lyophilized for further analysis.

The morphology and size of the MC were determined via transmission electron microscopy (TEM, Hitachi HT7700, Japan) and atomic force microscopy (AFM, Bruker Dimension Icon, Germany). MC (50 mg/L) were dissolved in deionized water, followed by gentle sonication in an ice water bath at 100 W for 15 min for TEM and AFM analyses. The organic and metal compositions of the MC were analyzed by X-ray photoelectron spectroscopy (XPS, K-Alpha, Thermo Fisher Scientific, MA) and inductively coupled plasma-mass spectrometry (ICP-MS, Agilent 7800) after wet digestion was performed using nitric acid and hydrogen peroxide (volume ratio = 4:1). Steady-state photoluminescence (PL) spectra and time-resolved PL spectra were obtained for lyophilized samples using an Edinburgh FLS1000/FS5 spectrophotometer. Elemental analyses (C, H, N, O, and S) were performed using a Vario CHO analyzer (Elementar, Germany) with 10 mg of lyophilized sample. The time−current (I−t) curve was determined using an electrochemical workstation (Chenhua, Inc., Shanghai, China) with controlled illumination (100 mW/cm^2). MC (10 mg/L) were coated on a glassy carbon electrode with 10% Nafion solution and served as the working electrode. An Ag/AgCl electrode was used as the reference electrode, and a Pt plate was used as the counter electrode. The photocurrent was measured in the ON and OFF states with a photon off/on shutter duration of 120 s. The UV−vis diffuse reflectance spectral features were recorded on a UV−vis spectrophotometer (UV-3600, Shimadzu, Japan) coupled to an integration sphere with $BaSO_4$ as a reference.

Culture Methods and Experimental Design. The marine cyanobacterium *T. erythraeum* strain IMS101 was obtained from the Center for Collections of Marine Algae (CCMA) of the State Key Laboratory of Marine Environmental Science (Xiamen University, China). The strain was originally isolated from the North Atlantic Ocean in 1993[27] and subsequently grown in artificial seawater (Table S1) enriched with YBC-II medium (Table S2).[28] Cultures were grown in triplicate using a dilute semicontinuous culture method at 26 °C in an incubator. The light intensity was 150 μmol photons/m^2/s, and the light/dark cycle was 14/10 h. All media were buffered with 25 μM ethylenediaminetetraacetic acid (EDTA) and passed through Chelex 100 resin (Bio-Rad Laboratories, CA) to remove Fe.[29]

Given that Fe released from MC may have a positive effect on *T. erythraeum*, the level of released Fe ions was monitored (Text S1). Approximately 20 nmol/L Fe ions were released after 72 h, as shown in Figure S2. Therefore, MC were used in the experiment at an environmentally relevant concentration (2.0 mg/L) with two different Fe concentrations (control: Fe-sufficient at 0.4 μmol/L; LFe: Fe-limited at 20 nmol/L released from MC). In addition, the amounts of inorganic nutrients (C, N, and P) released were measured to evaluate the effect of nutrient inputs (Text S1).

Determination of the Specific Growth Rate and Chlorophyll *a* Content. Cultures of *T. erythraeum* were grown in 1 L polycarbonate bottles at an initial cell density of 1 × 10^4 cells/mL. The detailed timeline of the experimental procedure is shown in Figure S3. The growth rate and chlorophyll *a* (Chl *a*) concentration were determined at the midpoint of the photoperiod from days 3 to 7 in the exponential growth phase. Cell counts were determined using an optical microscope (IX71, Olympus, Japan). Moreover, the optical density of the cells was assessed at 750 nm (OD_{750}) using a UV−Vis spectrophotometer (TU-1900, Purkinje General Instrument, China). The linear regression equation between OD_{750} and cell density was obtained during the exponential growth phase. The specific growth rates (μ) were calculated using the equation $\mu = (\ln N_1 - \ln N_0)/t$, where N refers to cell density and t is time in days. The filament length of *Trichodesmium* was obtained by measuring the length of the filaments on day 4 via confocal laser scanning fluorescence microscopy (CLSM, LSM880 with Airyscan, ZEISS, Germany). The concentration of Chl *a*, an indicator of biomass, was determined by 90% methanol extraction, followed by heating in a water bath at 65 °C for 6 min.[29] The extracts were centrifuged at 6000*g* for 10 min, and the absorbances of the supernatants were recorded at 650 nm (A_{650}), 665 nm (A_{665}), and 750 nm (A_{750}). The content of Chl *a* was calculated using the following equation.[29]

$$\text{Chl } a\ (\mu\text{g/mL}) = 16.5 \times (A_{665} - A_{750}) - 8.3 \times (A_{650} - A_{750})$$

The ATP, NADPH, and protein contents were measured with an ATP assay kit, a NADPH assay kit, and a protein assay kit, respectively. The instructions of the assay kit were strictly followed for all of the procedures (Beyotime Biotechnology, Shanghai, China) according to the manufacturer's instructions. The primary carbon-fixing enzyme ribulose 1,5-bisphosphate carboxylase/oxygenase (RuBisCo) for carbon assimilation was determined using an enzyme-linked immunoassay (ELISA) kit (MM-0602O1, Meimian, China) according to the manufacturer's protocols (Jiangsu Meimian Industrial Co., Ltd., China).

https://doi.org/10.1021/acs.est.4c01849
Environ. Sci. Technol. 2024, 58, 9236−9249

Measurement of Chlorophyll Fluorescence. The chlorophyll fluorescence parameters for photosystem II (PSII) were measured using a water chlorophyll fluorescence spectrometer (Walz, Water-PAM, Germany) and analyzed with WinControl-3 software. Prior to testing, the cells were incubated for 5 min in the dark. Blue light (440 nm) was selected for measurement, and the actinic light level was set to 400 μmol photons/m^2/s. Briefly, dark-adapted samples were induced by light (440 nm) to determine the minimum fluorescence yield (F_o). Subsequently, the maximum fluorescence yield (F_m) was detected during the first saturation pulse. The effective photochemical quantum yield of PSII (F_v/F_m) was calculated using the equation $F_v/F_m = (F_m - F_o)/F_m$.

The relative electron transport rate (rETR) was determined using the same samples at different light intensities. Light−response curves were recorded under stepwise increasing light intensity (0, 10, 20, 50, 100, 200, 500, and 1000 μmol photons/m^2/s), and the rETR was calculated as described previously.[30]

Electron Microscopy. For electron microscopy, cell cultures were collected by centrifugation (3000*g*, 10 min) and rinsed three times with 0.1 M phosphate-buffered saline (PBS). Then, the cells were immediately fixed in a mixture of freshly prepared aldehydes (4% paraformaldehyde and 2.5% glutaraldehyde, v/v = 1:1) in 0.1 M PBS overnight at 4 °C. The detailed protocols for preparing ultrathin sections are available in Text S2.

N_2 Fixation Rate and Ammonia Assimilation. The rate of N_2 fixation (nitrogenase activity) by *T. erythraeum* cells was measured using an acetylene reduction assay (ARA).[31] Cell culture samples (5 mL) were placed in 12 mL Labco vials (Exetainer, Labco, U.K.). One milliliter of air was extracted from the vial by a syringe, and then 1 mL of acetylene was injected into the headspace before incubation. The vials were incubated in the middle of the photoperiod for 2 h in a light growth chamber at 26 °C. A 500 μL aliquot of headspace gas was sampled and analyzed using a gas chromatograph (GC, Agilent 7890) equipped with a flame ionization detector. The GC was equipped with an HP-PLOT Q column (30 m × 0.32 mm, 40 μm) (Agilent Technologies, CA). The carrier gas was nitrogen at a pressure of 1.5 mL/min, and the injection and detector temperatures were 120 and 220 °C, respectively. The production of ethylene in the headspace was calculated using the Bunsen gas solubility coefficient[32] and a ratio of 4:1 to convert ethylene production rates to N_2 fixation rates. Glutamine synthetase (GS) and glutamine oxoglutarate aminotransferase (GOGAT) levels were determined using a GS assay kit (G0401W) and a GOGAT assay kit (GOGAT-1-Y), respectively, according to the manufacturer's protocols (Suzhou Grace Biotechnology Co., Ltd., China). The contents of 2-oxoglutarate (2-OG) and glutamate (Glu) were determined using commercially available assay kits (BC5425 and BC1585) according to the manufacturer's instructions (Solarbio Bioscience & Technology Co., Ltd., Shanghai, China).

AFM Probing of the Interactions between *T. erythraeum* and Marine Colloids. The details of the AFM imaging procedure are provided in Text S3 in the Supporting Information.

NanoSIMS Imaging. Stable isotope incubations were performed with ^{15}N ($^{15}N_2$, 99%, Wuhan Isotope Technology Co., Ltd., China). *T. erythraeum* was incubated for 48 h in YBC-II medium in a 100 mL headspace bottle, and 6 mL of $^{15}N_2$ gas was injected through the septum using a gastight syringe. For each treatment, 50 mL aliquots were filtered through a 1 μm polycarbonate membrane (Millipore) and fixed with 2.5% microscopy-grade glutaraldehyde overnight for NanoSIMS analyses. Then, the cells were rinsed twice with Milli-Q water to prevent salt crystals from forming during cell imaging. A 10 μL aliquot of cell suspension was dropped on a clean silicon chip (circle, diameter: 10 mm) and air-dried at ambient temperature. The dried samples were subsequently vacuumed and metalized by sputter deposition of a gold film (20 nm thickness) prior to analysis.

The ion images of the elements were analyzed on a NanoSIMS 50 L (CAMECA, Gennevilliers, France) instrument operated at the School of Earth System Science, Tianjin University. The samples were presputtered with a 1 nA Cs+ current for 2 min in a 45 × 45 μm^2 raster to remove gold and surface contaminants and reach the steady state of ion formation. NanoSIMS analyses were performed using a 0.7 pA 16 keV Cs+ primary ion beam, and data were collected for masses of $^{12}C^-$, $^{12}C^{14}N^-$, $^{12}C^{15}N^-$, and $^{56}FeO^-$. Target areas of *Trichodesmium* filaments were scanned on a 256 × 256 pixel raster with a raster area of 40 × 40 μm^2 and a counting time of 5000 μs/pixel. The negative secondary ions $^{12}C^-$, $^{12}C^{14}N^-$, $^{12}C^{15}N^-$, and $^{56}FeO^-$ were detected with electron multiplier detectors, and the secondary electrons were simultaneously imaged. These images were used to define regions of interest (ROIs). The mass resolving power for isobaric interferences was 6000−7000. Ratio images were obtained by dividing one mass image by another (e.g., $^{12}C^{15}N^-/^{12}C^{14}N^-$) and processed using the OpenMIMS plugin (https://github.com/BWHCNI/OpenMIMS) within ImageJ software.[33,34]

ESR Measurements. The generation of free radicals was recorded using a Magnettech MiniScope 400 ESR spectrometer (Magnettech, Germany) operated at a microwave frequency of 9.43 GHz and a magnetic field modulation frequency of 100 kHz.[35] Briefly, the production of $^{\bullet}OH$ in a colloid solution (50 mg/L) was probed by 5,5-dimethyl-1-pyrroline N-oxide (DMPO). The photoelectron and $^1O_2$ contents were monitored using 2,2,6,6-tetermethylpiperidine-N-oxyl (TEMPO) and 2,2,6,6-tetramethyl-4-piperidone (TEMP) as spin-trapping agents, respectively.

Cyclic Voltammetry Analysis. Cyclic voltammetry (CV) was employed to evaluate the capacity of *T. erythraeum* to accept electrons from MC. The peak potential (E_p) refers to the potential at which the current reaches a maximum (or minimum) during an electron transfer event. After 48 h of cultivation, the cell cultures were centrifuged at 3000*g* for 20 min and rinsed twice with 0.1 M PBS. The cyanobacterial cells were normalized to 5 × 10^4 cells/mL by resuspension in 0.1 M PBS. A 10 μL sample aliquot (MC coated with 10% Nafion, 10 mg/L) was dropped on the conductive side of a 1 cm^2 indium tin oxide (ITO) electrode and then dried at room temperature. CV analysis was conducted using a three-electrode system with an as-prepared ITO working electrode, a platinum electrode, and a Ag/AgCl reference electrode. CV curves were acquired using an electrochemical workstation (Chenhua, Inc., Shanghai, China) in the potential range between −0.60 and 0.60 V at a scan rate of 5 mV/s with 20 mL of cyanobacterial cell suspension. The visible light source was a 300 W xenon lamp with a cutoff filter (>420 nm) at a power density of 100 mW/cm^2.

Investigation of the Electron Transfer Pathway in *T. erythraeum*. The contribution of photoelectrons from MC to

https://doi.org/10.1021/acs.est.4c01849
Environ. Sci. Technol. 2024, 58, 9236−9249

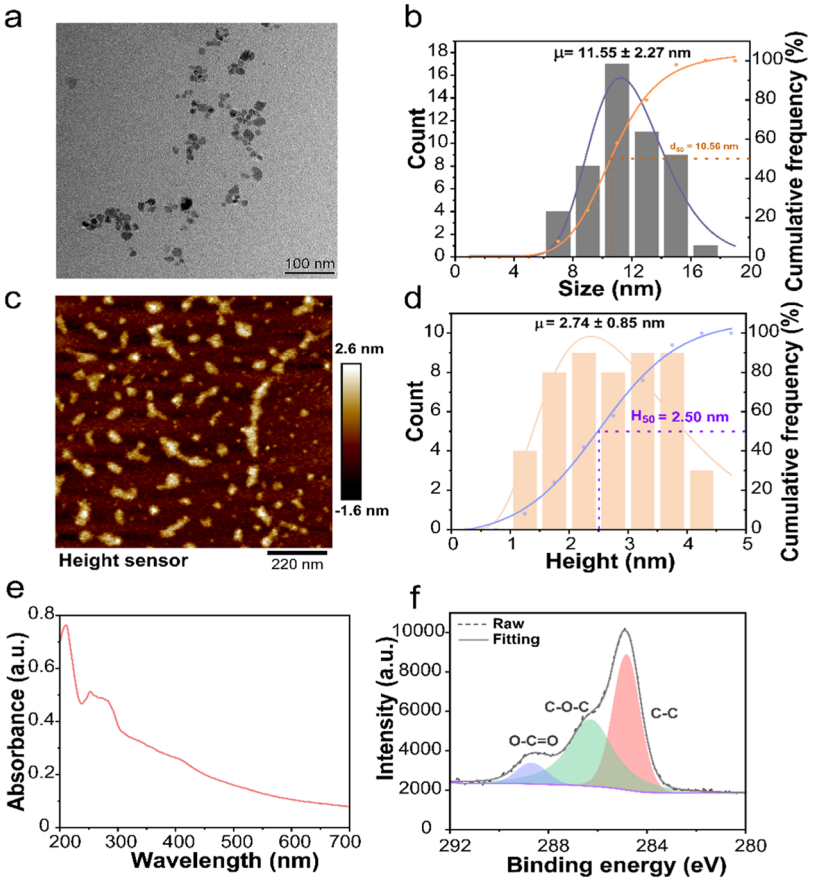

Figure 1. Characterization of marine colloids. (a, b) Representative TEM images of marine colloids and analysis of the size distribution (n = 50). (c, d) Typical AFM images of marine colloids and analysis of the height distribution (n = 50). (e) UV−vis absorption spectra of marine colloids. (f) XPS spectra showing C 1s peaks in marine colloids. The value of μ indicates the average size and height. D_{50} and H_{50} represent the value of the particle diameter/height at 50% in the cumulative distribution, respectively.

nitrogen fixation and assimilation was validated by adding silver nitrate ($AgNO_3$, an electron scavenger) to cell cultures. 3-(3,4-Dichlorophenyl)-1,1-dimethylurea (DCMU) blocks the plastoquinone binding site of PSII, preventing electron flow from PSII to plastoquinone.[36] In the nitrogenase system, the Fe protein cycle involves a transient association between the reduced, MgATP-bound Fe protein and the MoFe protein and includes electron transfer, ATP hydrolysis, the release of Pi, and the dissociation of the oxidized, MgADP-bound Fe protein from the MoFe protein.[37,38] MgATP hydrolysis has been proposed to be absolutely required for electron transfer from the Fe protein to the MoFe protein. *T. erythraeum* cells ($\sim 10^5$ cells/mL) were cultivated with 2.0 mg/L MC in the absence or presence of $AgNO_3$ (2 μM), DCMU (20 μM), or MgATP (0.5 mM). After 96 h of incubation, the ammonia content was measured with an ammonia assay kit (BC1525) according to the manufacturer's instructions (Solarbio Bioscience & Technology Co., Ltd., Shanghai, China).

Metabolomic and Transcriptomic Analysis. Subsamples from each culture flask (250 mL) were filtered through polycarbonate filters (25 mm, 3 μm, Millipore). The filters were immediately flash-frozen and stored in liquid nitrogen until extraction. Metabolites were extracted using liquid−liquid extraction, as described in Text S4. Transcriptomic analysis was performed at Tianjin Novogene Bioinformatics Technology Co., Ltd. The procedures used for RNA sequencing and DEG data analysis are provided in Text S5.

Quantitative Polymerase Chain Reaction Analysis. The relative transcript abundances of key genes encoding iron-containing protein constituents and exhibiting chlorophyll, ATPase, and nitrogenase activity were quantified via quantitative polymerase chain reaction (qPCR). The primer and probe sequences of the targeted genes are listed in Tables S3 and S4. More details on the RNA extraction and qPCR analysis methods used are provided in Text S6.

Statistical Analysis. At least three replicates of each culture condition were used in all of the experiments, and the data are expressed as the mean ± standard deviation (SD). One-way analysis of variance (ANOVA) with Tukey's multiple comparison test ($p < 0.05$) was used to determine significant differences. The normality (Shapiro−Wilk test) and homogeneity (Levene's test) of variance of the data were verified prior to analysis. All of the statistical analyses were performed with IBM SPSS Statistics 22.0, and the graphs were constructed using GraphPad Prism 8 and Origin 2023.

RESULTS AND DISCUSSION

Photoelectrochemical Properties of Marine Colloids. Natural colloids are abundant in oceans and are mainly composed of natural organic matter and mineral particles, with trace amounts of metals.[17,39] The concentration of MC extracted from Bohai Sea surface water using cross-flow ultrafiltration was 2.65 ± 0.28 mg/L. TEM and AFM confirmed the flake-like nanoscale shape of MC (Figure 1a−

https://doi.org/10.1021/acs.est.4c01849
Environ. Sci. Technol. 2024, 58, 9236−9249

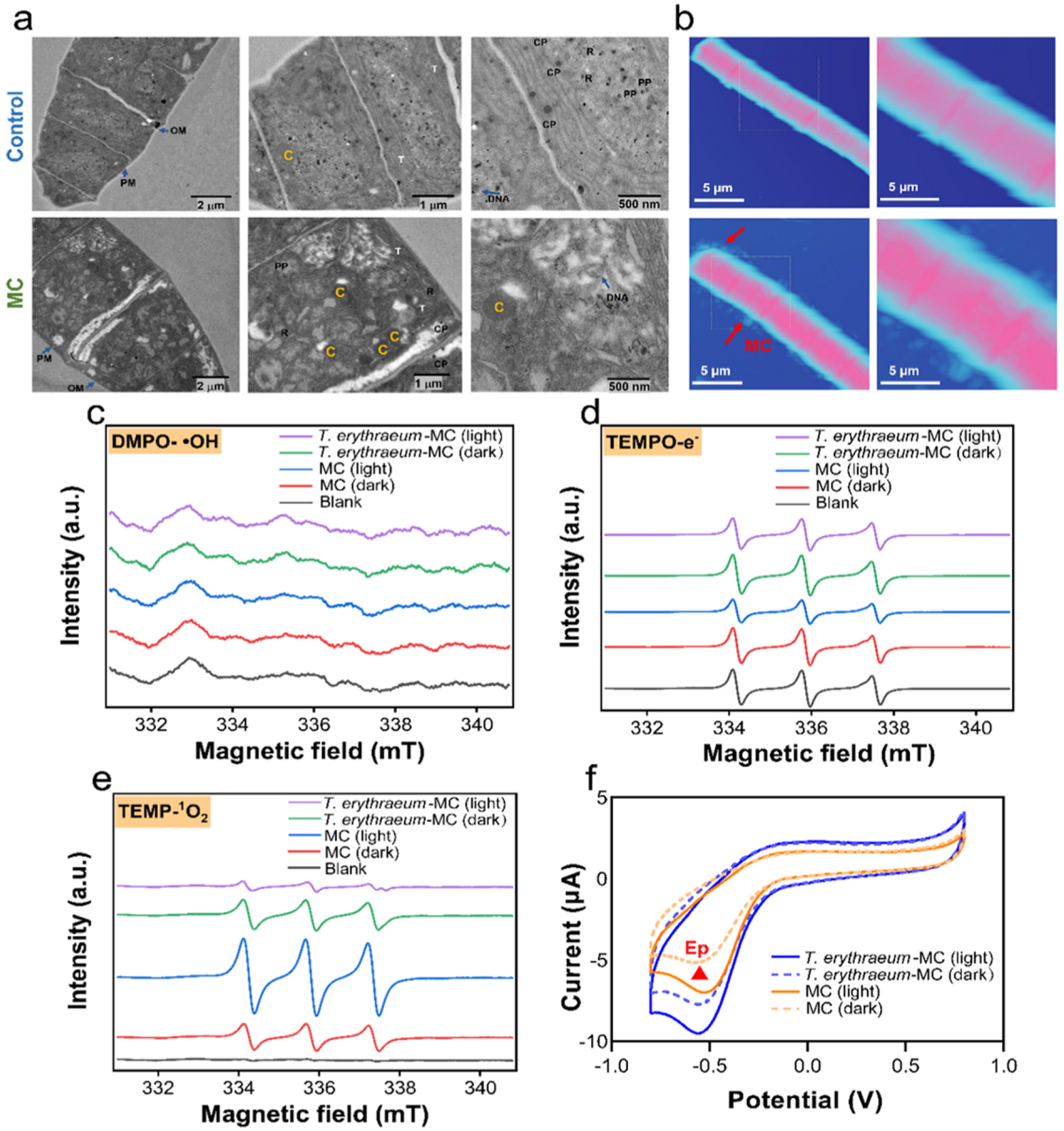

Figure 2. Electron transfer from marine colloids to *T. erythraeum*. (a) Electron micrograph of the ultrastructure of *T. erythraeum*. T, thylakoid membrane; C, carboxysome; CP, cyanophycin granule; PP, polyphosphate granule; R, ribosome; PM, plasma membrane; OM, outer membrane. (b) AFM images probing the interactions between *T. erythraeum* and marine colloids. (c–e) ESR spectra of •OH, electrons, and $^1O_2$ trapped by DMPO, TEMPO, and TEMP as spin probes, respectively. The blank samples are the ESR features of the spin-trapping agents. (f) Current response of marine colloids in 0.1 M PBS.

d). The lateral sizes of MC were 11.55 ± 2.27 nm (Figure 1c), and the thicknesses were approximately 1–5 nm (Figure 1d). The natural transformation of metal ions into metal nanoparticles occurs in a sunlit DOM-rich aqueous environment.[40] Complexation with ions or molecules can lead to the formation of nanoclusters, which may contribute to the photoelectrochemical characteristics of MC at the nanoscale.[41,42] MC exhibited two UV absorption peaks at 211 and 252 nm, which were attributed to the $\pi-\pi^*$ transition of the C=C band from the benzene ring and phenolic moieties (Figure 1e).[43,44] The phenolic moieties in DOM are linked to their electron-donating properties in oxidation reactions.[45] As shown in Figure S4, the light-triggered current of MC was approximately 0.0259 $\mu A/cm^2$, which was lower than that of common semiconductors (e.g., CdS and TiO_2).[46,47] Typical chromophores, e.g., carboxyl and carbonyl groups, were observed in the X-ray photoelectron C 1s spectrum (Figure 1f), contributing to the generation of a photocurrent in MC. The proportions of the chemical components of MC, including organic components (e.g., C, H, N, and S) and metal elements (e.g., Ca, Na, Mg, Al, and K) (Figure S5), were detected via elemental analysis and ICP-MS, respectively. The results confirmed that MC produced a relatively stable photocurrent, probably due to the mixture of organic–inorganic hybrids.[21] MC mixed organic and inorganic components at the nanometer scale, making it possible to obtain tailored optical and electronic properties and build electrical connections with living organisms.[48]

Marine Colloids Acting as Electron Donors for *T. erythraeum*. Marine DOM may serve as an important reservoir of C, N, and P and promote the growth of *T. erythraeum*.[49] However, during culture experiments, MC

https://doi.org/10.1021/acs.est.4c01849
Environ. Sci. Technol. 2024, 58, 9236–9249

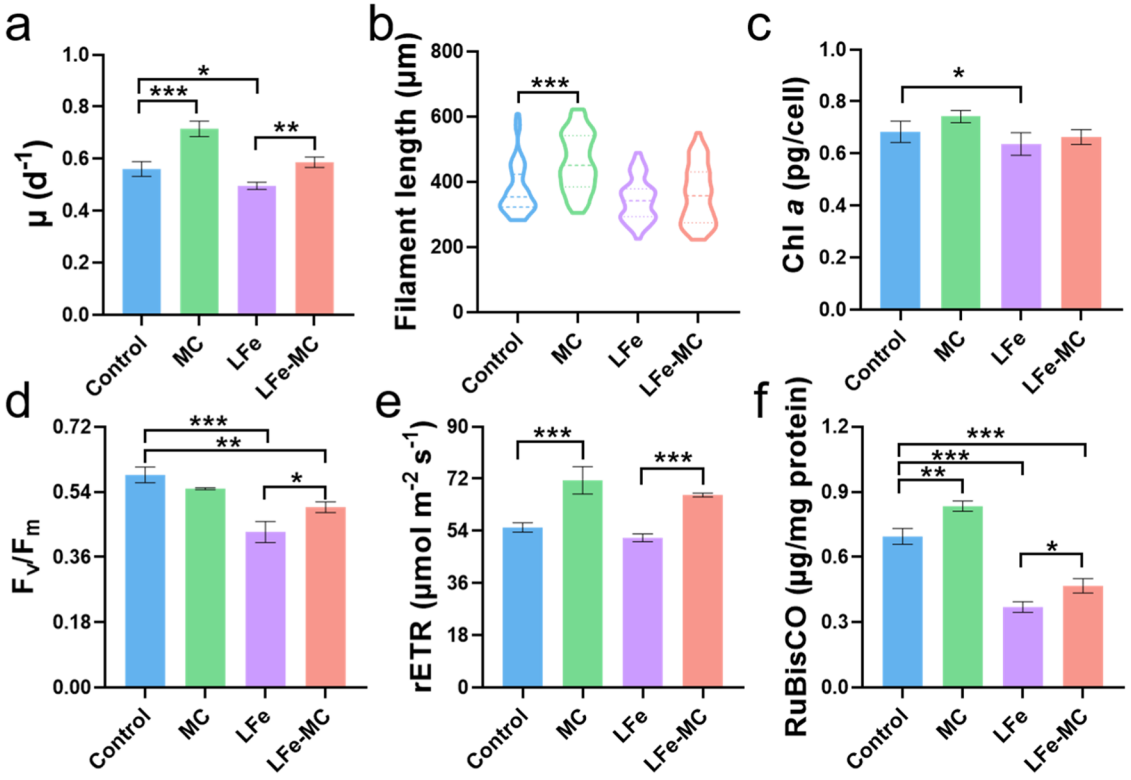

Figure 3. Cell growth and photosynthesis. (a) Growth rates of *T. erythraeum*. (b) Filament length (n = 50). (c) Chl *a* concentration. (d, e) Chlorophyll fluorescence parameters (F_v/F_m and rETR). (f) Content of RuBisCO available for CO_2 fixation Control: Fe at 0.4 μmol/L; MC: marine colloids at 2.0 mg/L, Fe at 0.4 μmol/L; LFe (Fe at 20 nmol/L); LFe-MC (marine colloids at 2.0 mg/L, Fe at 20 nmol/L). Asterisks indicate statistical significance: *p < 0.05, **p < 0.01, and ***p < 0.001.

exhibited a low dissolved total carbon concentration (0.73 ± 0.03 μM) and a low inorganic nutrient concentration. The concentrations of dissolved total nitrogen and dissolved total phosphorus were 0.07 μM and below the detection limit (0.02 μM), respectively. The above results were consistent with the finding that natural colloids are very stable in aquatic environments.[17,26] Therefore, as a nutrient source, MC had little effect on the growth of *Trichodesmium*. DOM can be directly taken up by *Trichodesmium* or primarily consumed by heterotrophic epibiont bacteria that ultimately transfer reduced DOM compounds to their host trichomes.[50] Therefore, the uptake of MC by *T. erythraeum* was evaluated by TEM. However, the cellular uptake of MC was not observed via TEM (Figure 2a). The absorption of MC on the cell surface was observed via AFM (Figure 2b). MC were mostly located in the extracellular space and tended to attach to the cells' outer membrane. Recent work has provided evidence that photoelectrotrophic denitrification occurs between DOM and *Thiobacillus denitrificans*.[22] As MC contain semiconducting minerals and chromophoric organic matter, marine nitrogen fixers (diazotrophs) may be affected by MC via electron transfer coupling, as verified below.

Colloids can be photosensitized to produce reactive oxygen species (e.g., $^{\bullet}OH$ and $^1O_2$) after irradiation with light.[21] A characteristic peak with an intensity ratio of 1:2:2:1 assigned to the DMPO-$^{\bullet}OH$ adduct was detected (Figure 2c). However, nearly no $^{\bullet}OH$ was found when DMPO was used as the trapping agent. As a spin-label molecule, TEMPO has a stable triplet ESR spectrum, and the signal with an intensity of 1:1:1 is weak after the reaction of TEMPO with electrons. After irradiation with MC, the ESR signal intensity of TEMPO (intensity ratio, 1:1:1) was reduced by 33.4 ± 1.75% compared with that of the excited photoelectrons (Figure 2d). $^1O_2$ is a nonmagnetic molecule and cannot be detected directly by electron paramagnetic resonance (EPR). However, the reaction between $^1O_2$ and TEMP produces the free radical TEMPO, which is a proxy for $^1O_2$. Photogenerated electrons and $^1O_2$ produced from MC were reduced after the reaction with *T. erythraeum* (Figure 2d,e). The CV reduction peak of MC was observed at E_p = −652 mV (cathodic versus Ag/AgCl) (Figure 2f). Compared with the control electrode coated with MC, *T. erythraeum* resulted in a decreased reduction in current, indicating that at a given voltage, less electrical charge passed through the cyanobacterial cells. In other words, *T. erythraeum* showed a high capacity to receive photogenerated electrons from the MC. Moreover, the photoelectrons produced from MC were captured by *T. erythraeum*, thereby inhibiting the generation of $^1O_2$ from reduced superoxide anions ($^{\bullet}O_2^-$). Natural minerals can produce photoexcited electrons upon irradiation, and the photoelectrotrophic effects were found to greatly enhance carbon fixation.[51,52] However, the natural photoelectrophy pathway driven by MC has not received much attention until now.

Promotion of the Electron Transfer Rate in Photosynthesis by Marine Colloids. During the growth phase, the cell biomass gradually increased with increasing MC concentration (0.2−20 mg/L) (Figure S6). MC promoted the growth of *T. erythraeum* under Fe-sufficient and Fe-limited conditions (Figure 3a), resulting in ∼27.4% faster growth of Fe-sufficient cells (p < 0.001) and ∼18.2% faster growth of Fe-limited cells (p < 0.01). The filament length of the Fe-limited

https://doi.org/10.1021/acs.est.4c01849
Environ. Sci. Technol. 2024, 58, 9236−9249

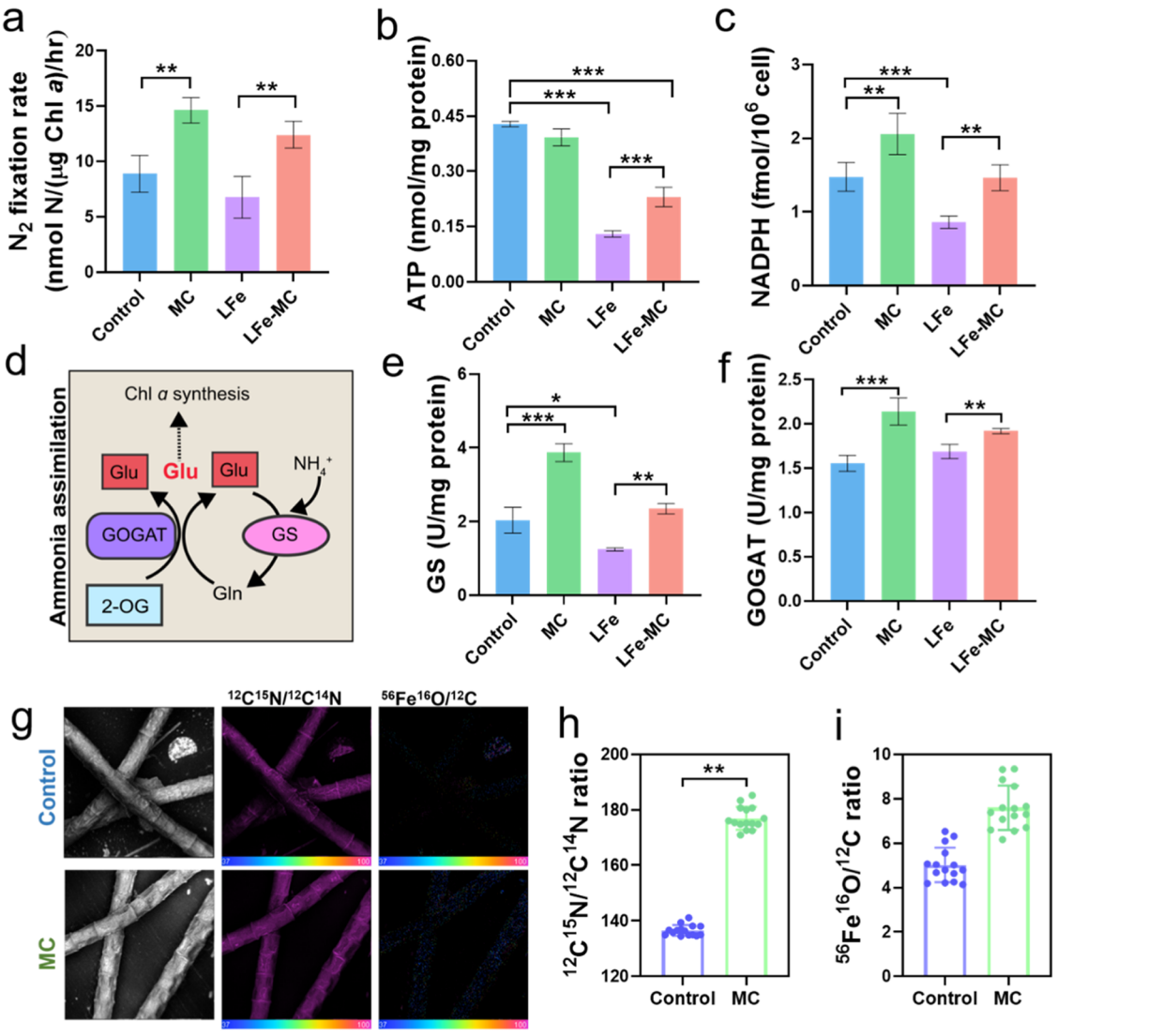

Figure 4. Enhanced N_2 fixation by marine colloids. (a) N_2 fixation rate. (b) Intracellular ATP content. (c) Intracellular NADPH content. (d) Diagram of ammonium assimilation catalyzed by the GS−GOGAT cycle in *T. erythraeum*. Gln, glutamine. (e, f) GS and GOGAT activity. (g) Representative NanoSIMS images of *T. erythraeum*. (h, i) Calculations of ^{12}C $^{15}N/^{12}C$ ^{14}N and $^{56}Fe^{16}O/^{12}C$ derived from NanoSIMS images (n = 15). Asterisks indicate statistical significance: *p < 0.05, **p < 0.01, and ***p < 0.001.

cells was shorter than that of the control cells (Figure 3b), which was consistent with decreased growth in response to Fe limitation.[11,12] After MC treatment, the filament length of *T. erythraeum* increased by 28.7% (p < 0.001) and 30% (p = 0.76) in the Fe-sufficient and Fe-limited cultures, respectively. Thus, MC induced a significant increase in filament length in *T. erythraeum* compared to that in the control (p < 0.05). As shown in Figure 3c, the Chl *a* content was significantly lower by 50% in Fe-limited cells than in Fe-sufficient cells (p < 0.05). Reduced Chl *a* synthesis is a hallmark of Fe deficiency in cyanobacteria.[11] The average F_v/F_m of the Fe-limited group was reduced by 26.9% (Figure 3d) compared with that of the control group. In contrast, the F_v/F_m significantly increased in response to MC under Fe-limited conditions (p < 0.05), which was consistent with the increase in growth rate.

The rETR is the product of the effective photochemical yield of PSII. Fe limitation drastically decreased electron transport in marine cyanobacteria.[11,53] Figure 3e shows that the rETR increased significantly with the addition of MC to both Fe-sufficient cells and Fe-limited cells. The content of the CO_2-fixation enzyme RuBisCO, which is encapsulated in carboxysomes, increased by 20.1% in the presence of MC compared to that in the control (Figure 3e). MC induced a notable increase in the RuBisCO content in Fe-limited cells, approximately 126% of that in Fe-limited cells alone. In the control and MC groups, the cyanobacterial cells exhibited complete cell walls, cell membrane structures, and regularly organized thylakoid membrane lamella (Figure 3f). Abundant carboxysomes provide elevated levels of CO_2 around RuBisCO to increase CO_2 fixation in cyanobacteria.[54] The percentage of carboxysomes was higher in the MC-treated cells than in the control cells (Figure S7), which was consistent with the increased contents of Chl *a* and RuBisCO. These results suggested that MC significantly promoted the growth and photosynthetic electron transfer rate of *T. erythraeum* by increasing the Chl *a* and RuBisCO contents.

Transfer of Photoelectrons to the PET Chain Facilitated Nitrogen Fixation and Assimilation. MC significantly increased the N_2 fixation rate in both Fe-sufficient cells (67.4 ± 21.5%, p < 0.01) and Fe-limited cells (89.3 ±

https://doi.org/10.1021/acs.est.4c01849
Environ. Sci. Technol. 2024, 58, 9236−9249

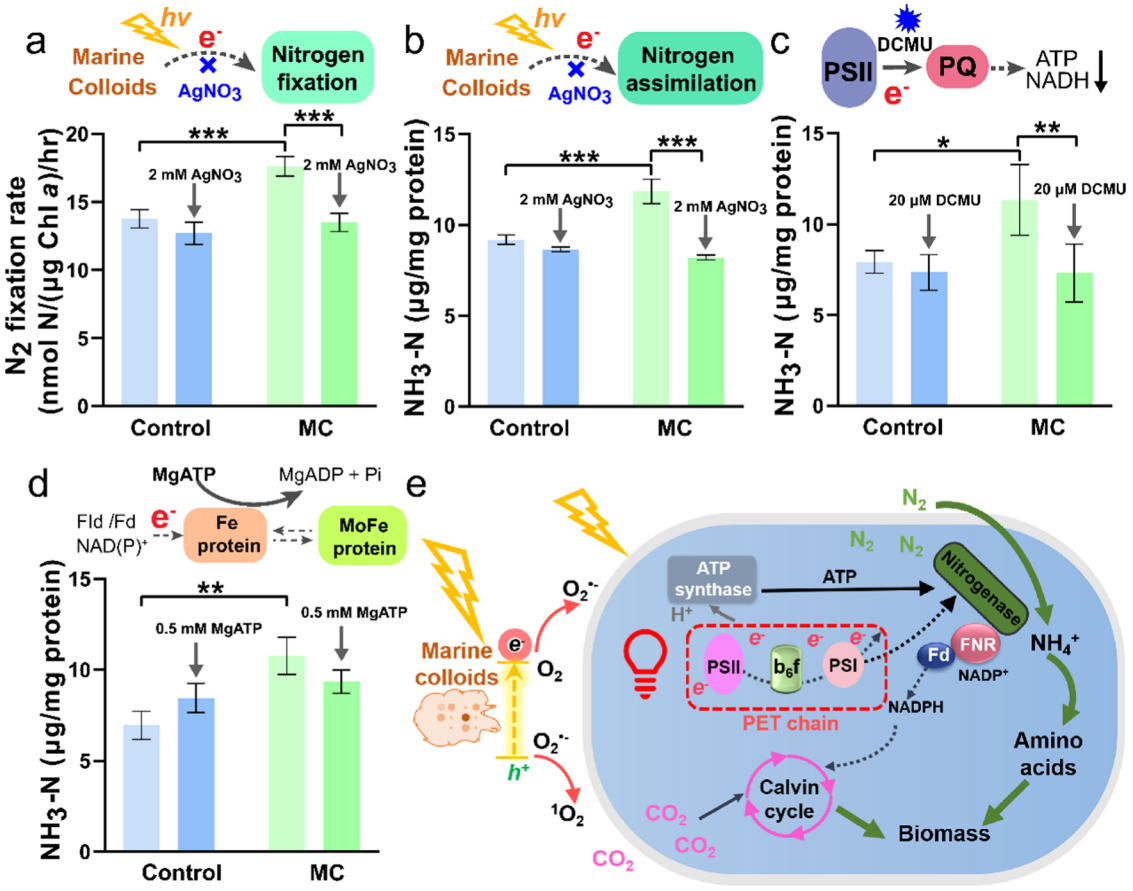

Figure 5. Photoexcited electrons from marine colloids integrated with the PET chain contribute to nitrogen assimilation. (a, b) N_2 fixation rate and NH_3−N production in *T. erythraeum* treated with or without 2 μM $AgNO_3$ after 96 h of incubation. (c) NH_3−N production in *T. erythraeum* treated with or without 20 μM DCMU after 96 h of incubation. (d) NH_3−N production in *T. erythraeum* treated with or without 0.5 mM MgATP after 96 h of incubation. (e) Proposed mechanism for enhanced nitrogen assimilation by marine colloids. PS I, photosystem I; b6f, 2-cytochrome b6f complex; Fd, ferredoxin; FNR, ferredoxin-NADP reductase. Asterisks indicate statistical significance: *$p < 0.05$, **$p < 0.01$, and ***$p < 0.001$.

31.0%, $p < 0.01$), as illustrated in Figure 4a. ATP is an essential assimilatory energy source for nitrogenase through the reduction of N_2 to NH_3 in *T. erythraeum*.[11,55] Low ATP availability was observed under Fe-limited conditions (Figure 4b) and might lead to low rates of nitrogenase activity. A high level of NADPH was observed during N_2 fixation in the MC-treated cells (Figure 4c), implying that excessive electrons were generated by ferredoxin-NADP+ oxidoreductase (FNR). MC improved the performance of nitrogenase and FNR, suggesting that more reducing powers were received from the PET chain by their common electron supplier, ferredoxin (Fd).[25]

As shown in Figure 4d, after atmospheric N_2 is fixed into ammonia by nitrogenase, ammonia is incorporated into the carbon skeleton by the sequential action of GS and GOGAT in cyanobacteria cells.[56,57] The activities of GS and GOGAT after treatment with MC greatly increased by 88.0−90.0 and 13.7−37.5% in Fe-sufficient cells and Fe-limited cells, respectively (Figure 4e,f). 2-OG is a key metabolite closely coupled to carbon and nitrogen metabolism, as well as the carbon skeleton substrate of the GS−GOGAT pathway.[56,58] MC significantly increased the content of 2-OG ($p < 0.05$) in Fe-limited cells (Figure S8). Furthermore, the abundance of Glu (the substrate for Chl *a* synthesis and the GS−GOGAT cycle) in Fe-limited cells may be significantly increased by MC, as verified by the increases in Chl *a* and N_2 fixation. NanoSIMS has become one of the most promising techniques for elemental imaging,[59,60] providing direct evidence for carbon and nitrogen assimilation in *Trichodesmium*. Compared with that in the control, the $^{12}C^{15}N/^{12}C^{14}N$ enrichment in *T. erythraeum* increased by 29.6 ± 3.23% ($p < 0.01$) in response to MC, while the accumulation of $^{56}Fe^{16}O/^{12}C$ increased by 52.0 ± 8.31% ($p > 0.05$) in cyanobacterial cells treated with MC (Figure 3g−i). The increases in ^{15}N enrichment were consistent with the increases in nitrogen fixation and ammonia assimilation promoted by MC. $AgNO_3$, a typical electron scavenger, was added to the *T. erythraeum*−MC system to quench photoelectrons.[61] After $AgNO_3$ was added, the N_2 fixation rate and NH_3−N production under light decreased to the same levels as those in the control (Figure 5a,b). The above results demonstrated the crucial role played by photoexcited electrons from MC in enhancing nitrogen fixation and assimilation, as bioavailable electron donors were provided to *T. erythraeum*.

The photoinduced electrons from CdS NPs and AuNPs can greatly augment photosynthesis by supplying exogenous electrons through the PET chain in photosynthetic bacteria, which then promotes renewable chemical production (e.g., hydrogen production and nitrogen fixation).[25,62] The photoinduced electrons from MC might integrate with the PET chain, thus generating excess intracellular reducing power for nitrogenase catalysis. The quinone pool is an important component of electron transfer across the membrane.[63] DCMU blocks cross-membrane electron transfer by inhibiting

https://doi.org/10.1021/acs.est.4c01849
Environ. Sci. Technol. 2024, 58, 9236−9249

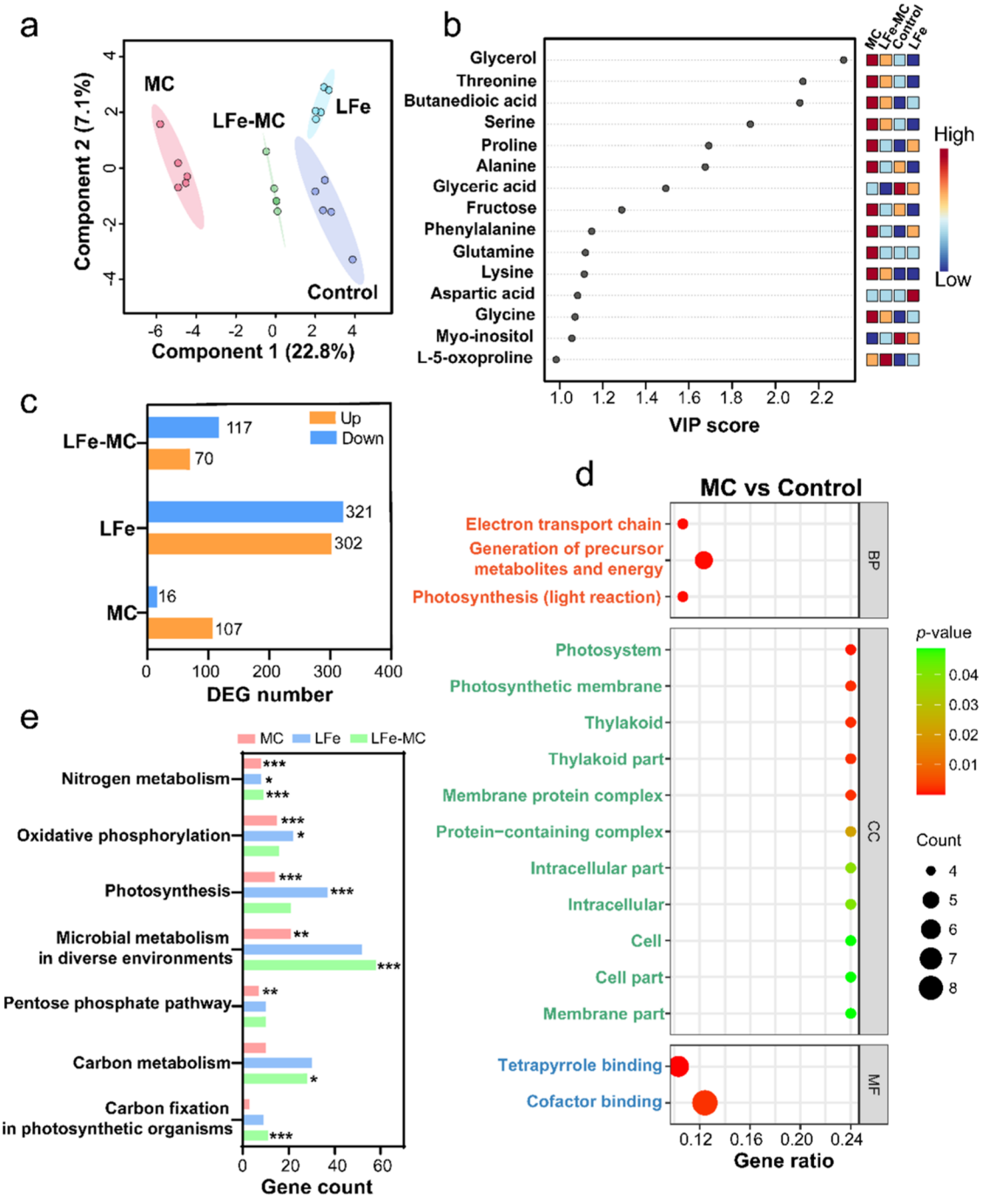

Figure 6. Metabolomic and transcriptomic analysis of *T. erythraeum*. (a) PLS-DA score plot of metabolomic data, illustrating a distinct separation among treatments. (b) Variable importance (VIP) score of the identified metabolites. Metabolites with VIP scores >1.0 were identified as contributory variables in the PLS-DA model. (c) Number of DEGs compared with the control. (d) GO term analysis of the significant enrichment of DEGs in *T. erythraeum* exposed to marine colloids (adjusted to $p < 0.05$) compared with those in the control group. The gene ratio indicates the ratio of the number of DEGs enriched in a GO term to the total number of DEGs. (e) Top 7 KEGG pathways with significant enrichment of DEGs in the MC, LFe, and LFe-MC groups compared with the control group. Asterisks indicate significantly enriched KEGG pathways: *$p < 0.05$, **$p < 0.01$, and ***$p < 0.001$.

the key enzyme (NAD(P)H:quinone oxidoreductase) shuttle of electrons flowing into the quinone pool in the inner membrane.[64] In cyanobacteria, NAD(P)H:quinone oxidoreductase can catalyze the two-electron reduction of quinones and plays a role in functions, such as respiration, cyclic electron flow around photosystem I, and CO_2 uptake.[65] A significant decrease of approximately 35.5% in NH_3-N production was observed upon the addition of DCMU compared with that in the inhibitor-free MC group (Figure 5c), suggesting that the involvement of the quinone pool in the PET chain is crucial for N_2 fixation in cyanobacterial cells treated with MC. Recent reports have shown that photoexcited electrons from colloidal quantum dots are directly transferred to the nitrogenases of N_2-fixing bacteria (*Azotobacter vinelandii*) to facilitate N_2 fixation.[66] Considering their similar nanostructure, we speculated that MC can replace the Fe protein to transfer

https://doi.org/10.1021/acs.est.4c01849
Environ. Sci. Technol. 2024, 58, 9236−9249

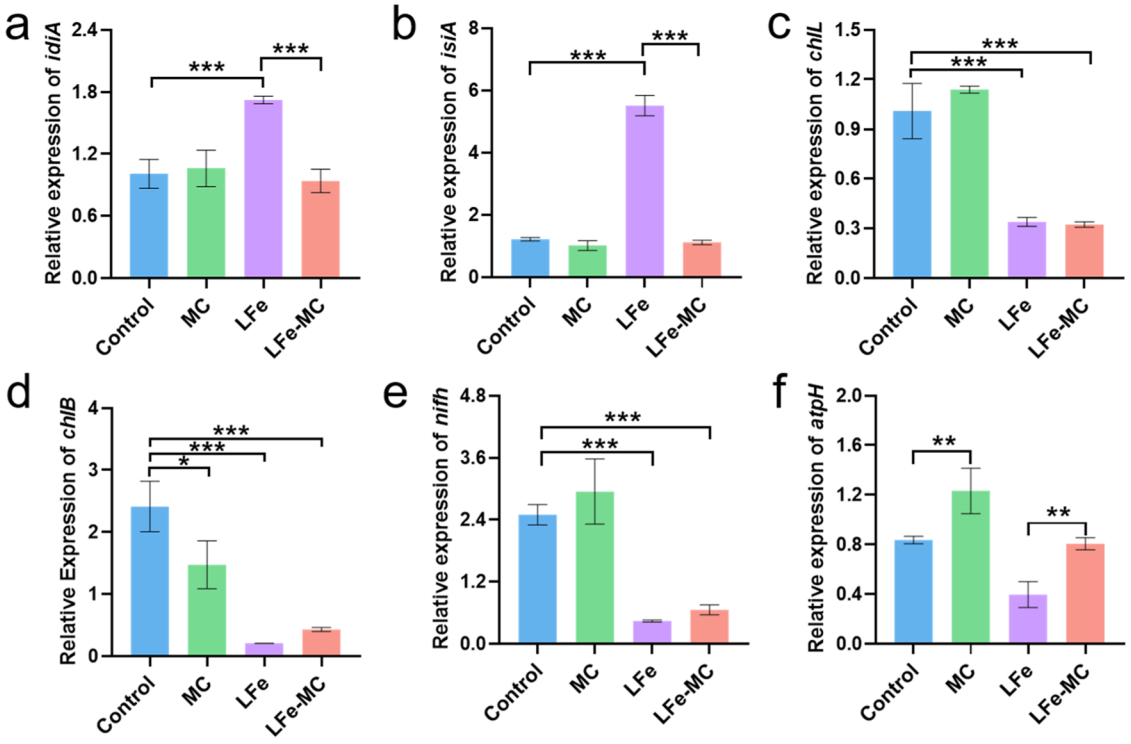

Figure 7. Transcript expression of key genes encoding iron-containing protein constituents, chlorophyll, nitrogenase activity, and ATPase. (a, b) Expression of the iron stress-related protein-encoding genes *idiA* and *isiA*. (c, d) Expression of genes involved in Chl *a* biosynthesis, *chlL* and *chlB*. (e) Expression of the gene encoding the nitrogenase iron protein *nifH*. (f) Expression of the ATPase subunit gene *atpH*.

electrons to the MoFe protein in *T. erythraeum*. However, that assumption was refuted by the AFM observations, which showed that MC absorbed on the cell surface and was not taken up by the cell directly. Alternatively, photoexcited electrons from MC may enhance the Fe protein cycle. In the nitrogenase system, MgATP can promote the nitrogenase Fe protein cycle by increasing the intracellular concentration of viable Fe protein.[38] Compared with the control, the addition of MgATP and MC increased the productivity of NH_3−N by 21.6 and 55.0%, respectively (Figure 5d). However, MgATP had no significant effect on NH_3−N production in the MC group. Specifically, the electron transfer between the Fe protein and the MoFe protein is not accelerated by MC. Therefore, photoexcited electrons are transferred from MC to *T. erythraeum* cells and increase the PET chain activity and nitrogen assimilation under light illumination (Figure 5e). Moreover, MC did not impair the photosynthetic system and effectively eliminated O_2 during the process of charge separation (Figure 5e). Since *T. erythraeum* is sensitive to oxygen, daytime nitrogen fixation must outweigh the costs involved in protecting the nitrogenase enzyme from degradation by oxygen.[5]

Underlying Mechanisms of Carbon and Nitrogen Metabolism Regulated by Marine Colloids. Metabolomic and transcriptomic analyses were performed to systematically explore the potential mechanisms underlying biological alterations in response to MC. As shown in Figure S9, 40 differentially abundant metabolites, including amino acids, fatty acids, small-molecule acids, and carbohydrates, were identified. The score plot of the partial least-squares discrimination analysis (PLS-DA) indicated an obvious separation of the treated groups from the control group (Figure 6a). Fifteen metabolites (e.g., glutamine, serine and phenylalanine) had variable importance in projection (VIP) scores greater than 1.0 (Figure 6b) and were involved mainly in ammonia assimilation and amino acid metabolism. As illustrated in Figure 6c, significant differences in the differentially expressed genes (DEGs) ($p < 0.01$ and $\log_2$-fold change >1) were observed between the MC-treated and Fe-limited cells. Furthermore, key genes linked to carbon and nitrogen metabolism were identified, including *psaA/psaC/psaJ/psbC/psbD/psbE/psaJ/petD/petE/petG*, which are related to photosynthesis (e.g., photosystem, cytochrome b6f complex, and PET), and *gln A/nifH/nifK/nifD/gltB*, which are linked to nitrogen fixation and ammonia assimilation. The identified genes were subjected to Gene Ontology (GO) and Kyoto Encyclopedia of Genes and Genomes (KEGG) pathway analyses. GO analysis indicated that MC had significant effects on the electron transport chain, the generation of precursor metabolites and energy, photosystems and photosynthesis, and tetrapyrrole binding ($p < 0.001$; Figure 6d). Fe is an essential metal necessary for N_2 fixation and photosynthesis,[11,67] since photosystems II and I and nitrogenases in *Trichodesmium* require 3, 12, and 19 Fe atoms, respectively. The processes related to photosynthesis (photosystems II and I) and respiratory electron transport metabolism were significantly affected ($p < 0.05$) under Fe-limited conditions (Figure S10). Consistently, the electron transport chain, generation of precursor metabolites and energy, photosystem and photosynthesis, and tetrapyrrole binding were upregulated by MC under Fe-limited conditions (Figure S11). Moreover, metabolic processes, including heterocycle biosynthetic processes, nucleobase-containing compound biosynthetic processes, and organonitrogen compound catabolic processes, were significantly enriched in the LFe-MC cells compared with the control cells (Figure S11).

https://doi.org/10.1021/acs.est.4c01849
Environ. Sci. Technol. 2024, 58, 9236−9249

MC significantly promoted photosynthetic electron transfer to supply energy for nitrogen fixation, which was also demonstrated via KEGG pathway analysis. The leading pathways enriched in genes upregulated by MC were involved in nitrogen metabolism, oxidative phosphorylation, photosynthesis, microbial metabolism in diverse environments, and the pentose phosphate pathway (Figure 6e). The DEGs in the LFe-MC group were most enriched in microbial metabolism in diverse environmental pathways, followed by nitrogen metabolism and carbon fixation ($p < 0.001$). The availability of Fe is critically important in determining nitrogen fixation rates and photochemical energy conversion efficiency.[9,11]

Transcripts of key genes that encode iron-containing protein constituents, chlorophyll, nitrogenase, and ATPase were confirmed by qPCR (Figure 7). Fe deficiency upregulated the expression of two major Fe stress biomarkers, *idiA* and *isiA*, whereas the transcription of *idiA* and *isiA* was downregulated by MC. Consistent with the decrease in the cellular content of glutamate (the substrate for Chl *a* synthesis), *chlL*- and *chlB*-related chlorophyll decreased significantly in response to Fe deficiency. The upregulation of *chlB* transcription by MC was also consistent with the increase in cellular Chl *a* content. Elevated transcription of the nitrogenase gene (*nifH*) and ATPase subunit gene (*atpH*) explained the increases in the N_2 fixation rate and ATP content in the presence of MC. RNA-Seq was further confirmed by qPCR analyses (Figure S12). Taken together, the above results revealed that the regulation of photosynthetic electron transfer and tetrapyrrole binding by MC contributed to increases in carbon and nitrogen fixation in *T. erythraeum*.

Environmental Implications. N_2 fixation is catalyzed by nitrogenase in diazotrophs and plays an important role in the global nitrogen cycle. As a diazotrophic cyanobacterium, *Trichodesmium* provides a valuable source of bioavailable N in N-limited regions.[68] Under visible light irradiation, MC exhibit photoelectrochemical properties and trigger the generation of electrons. Photoexcited electrons from MC facilitated electron transfer to increase the rate of photosynthesis and effectively increased N_2 fixation by 67.5−89.3%. Furthermore, *T. erythraeum* showed significantly upregulated expression of genes related to photosynthesis and photosynthetic electron transfer in the presence of MC. These findings reveal the overlooked role of MC in biological nitrogen fixation. Given the pivotal role of *Trichodesmium* in supplying new nitrogen in the ocean, MC exhibit great potential to increase nitrogen fixation, which has far-reaching implications for ocean biology and biogeochemistry.

N_2 fixation is an external source of "new" N in the upper ocean that plays a dominant role in the sinking and loss of N and associated C to the deep ocean.[69] As an uncertain method for relieving Fe stress, Fe fertilization in the low-nutrient and low-chlorophyll regions of the ocean to stimulate N_2 fixation could lead to the sequestration of atmospheric carbon, directly affecting atmospheric CO_2 dynamics and global climate change.[70] MC may provide an environmentally friendly strategy and exhibit great potential to enhance biological nitrogen fixation in surface environments. Our work describes a scenario, in which MC simultaneously enhanced nitrogen fixation and photosynthesis by promoting electron transfer in *Trichodesmium*. However, further research is needed to investigate the role of electron transfer in the enigma of simultaneous nitrogen fixation and oxygenic photosynthesis in *Trichodesmium*.[71,72]

This work provides solid evidence for the natural occurrence of photoelectrophy in marine ecosystems, in which broadly distributed cyanobacterial diazotrophs use electrons from MC for nitrogen and carbon fixation. In addition to nitrogen fixers, ammonia oxidizers and denitrifiers might have the potential to exhibit photoelectrophy, which would indicate that these processes are also affected by MC. Additional work to elucidate the effects of MC on the ocean element cycle should be done in the future.

■ ASSOCIATED CONTENT

Supporting Information

The Supporting Information is available free of charge at https://pubs.acs.org/doi/10.1021/acs.est.4c01849.

The detailed methods used for the experiments involving marine colloids, TEM and AFM images of *T. erythraeum* cells, metabolomic and transcriptomic analyses, and RNA extraction and qPCR analysis (Texts S1−S6); compositions of artificial seawater and YBC-II medium, genes and sequences of primers used for qPCR analysis (Tables S1−S5); and the results concerning inorganic and metal elements in marine colloids, contents of 2-OG and Glu, heatmaps of identified metabolites, GO term and KEGG pathway enrichment analysis of DEGs and validation of the RNA-Seq results using qPCR (Figures S1−S12) (PDF)

■ AUTHOR INFORMATION

Corresponding Author

Xiangang Hu − *Key Laboratory of Pollution Processes and Environmental Criteria (Ministry of Education), Carbon Neutrality Interdisciplinary Science Centre, College of Environmental Science and Engineering, Nankai University, Tianjin 300350, China;* orcid.org/0000-0002-9403-816X; Email: huxiangang@nankai.edu.cn

Authors

Weilu Kang − *Key Laboratory of Pollution Processes and Environmental Criteria (Ministry of Education), Carbon Neutrality Interdisciplinary Science Centre, College of Environmental Science and Engineering, Nankai University, Tianjin 300350, China*

Li Mu − *Tianjin Key Laboratory of Agro-Environment and Product Safety, Key Laboratory for Environmental Factors Controlling Agro-Product Quality Safety (Ministry of Agriculture and Rural Affairs), Institute of Agro-Environmental Protection, Ministry of Agriculture and Rural Affairs, Tianjin 300191, China*

Complete contact information is available at: https://pubs.acs.org/10.1021/acs.est.4c01849

Notes

The authors declare no competing financial interest.

■ ACKNOWLEDGMENTS

This work was financially supported by the National Natural Science Foundation of China (grant no. U22A20615 and 42077366) and the 111 Program (grant no. B17025). The first author, Weilu Kang, was funded by the Shanghai Tongji Gao Tingyao Environmental Science & Technology Development Foundation. The authors thank Kunshan Gao from Xiamen University for providing the cyanobacterium *Trichodesmium*.

REFERENCES

(1) Gruber, N.; Galloway, J. N. An Earth-system perspective of the global nitrogen cycle. *Nature* **2008**, *451*, 293−296.
(2) Sohm, J. A.; Webb, E. A.; Capone, D. G. Emerging patterns of marine nitrogen fixation. *Nat. Rev. Microbiol.* **2011**, *9*, 499−508.
(3) Hutchins, D. A.; Capone, D. C. The marine nitrogen cycle: new developments and global change. *Nat. Rev. Microbiol.* **2022**, *20*, 401−414.
(4) Bonnet, S.; Benavides, M.; Le Moigne, F. A. C.; Camps, M.; Torremocha, A.; Grosso, O.; Dimier, C.; Spungin, D.; Berman-Frank, I.; Garczarek, L.; Cornejo-Castillo, F. M. Diazotrophs are overlooked contributors to carbon and nitrogen export to the deep ocean. *ISME J.* **2023**, *17*, 47−58.
(5) Held, N. A.; Waterbury, J. B.; Webb, E. A.; Kellogg, R. M.; McIlvin, M. R.; Jakuba, M.; Valois, F. W.; Moran, D. M.; Sutherland, K. M.; Saito, M. A. Dynamic diel proteome and daytime nitrogenase activity supports buoyancy in the cyanobacterium *Trichodesmium*. *Nat. Microbiol.* **2022**, *7*, 300−311.
(6) Capone, D. G.; Burns, J. A.; Montoya, J. P.; Subramaniam, A.; Mahaffey, C.; Gunderson, T.; Michaels, A. F.; Carpenter, E. J. Nitrogen fixation by *Trichodesmium* spp.: An important source of new nitrogen to the tropical and subtropical North Atlantic Ocean. *Global Biogeochem. Cycles* **2005**, *19*, No. GB2024.
(7) Benavides, M.; Bonnet, S.; Le Moigne, F. A. C.; Armin, G.; Inomura, K.; Hallstrom, S.; Riemann, L.; Berman-Frank, I.; Poletti, E.; Garel, M.; Grosso, O.; Leblanc, K.; Guigue, C.; Tedetti, M.; Dupouy, C. Sinking *Trichodesmium* fixes nitrogen in the dark ocean. *ISME J.* **2022**, *16*, 2398−2405.
(8) Snow, J. T.; Schlosser, C.; Woodward, E. M. S.; Mills, M. M.; Achterberg, E. P.; Mahaffey, C.; Bibby, T. S.; Moore, C. M. Environmental controls on the biogeography of diazotrophy and *Trichodesmium* in the Atlantic Ocean. *Global Biogeochem. Cycles* **2015**, *29*, 865−884.
(9) Berman-Frank, I.; Cullen, J. T.; Shaked, Y.; Sherrell, R. M.; Falkowski, P. G. Iron availability, cellular iron quotas, and nitrogen fixation in *Trichodesmium*. *Limnol. Oceanogr.* **2001**, *46*, 1249−1260.
(10) Mark Moore, C.; Mills, M. M.; Achterberg, E. P.; Geider, R. J.; LaRoche, J.; Lucas, M. I.; McDonagh, E. L.; Pan, X.; Poulton, A. J.; Rijkenberg, M. J. A.; Suggett, D. J.; Ussher, S. J.; Woodward, E. M. S. Large-scale distribution of Atlantic nitrogen fixation controlled by iron availability. *Nat. Geosci.* **2009**, *2*, 867−871.
(11) Shi, T.; Sun, Y.; Falkowski, P. G. Effects of iron limitation on the expression of metabolic genes in the marine cyanobacterium *Trichodesmium erythraeum* IMS101. *Environ. Microbiol.* **2007**, *9*, 2945−2956.
(12) Küpper, H.; Setlik, I.; Seibert, S.; Prasil, O.; Setlikova, E.; Strittmatter, M.; Levitan, O.; Lohscheider, J.; Adamska, I.; Berman-Frank, I. Iron limitation in the marine cyanobacterium *Trichodesmium* reveals new insights into regulation of photosynthesis and nitrogen fixation. *New Phytol.* **2008**, *179*, 784−798.
(13) Rutledge, H. L.; Tezcan, F. A. Electron transfer in nitrogenase. *Chem. Rev.* **2020**, *120*, 5158−5193.
(14) Rucker, H. R.; Kaçar, B. Enigmatic evolution of microbial nitrogen fixation: Insights from Earth's past. *Trends Microbiol.* **2023**, No. S0966-842X(23)00091-4, DOI: 10.1016/j.tim.2023.03.011.
(15) Doney, S. C. Oceanography - Plankton in a warmer world. *Nature* **2006**, *444*, 695−696.
(16) Wang, W. X.; Guo, L. D. Influences of natural colloids on metal bioavailability to two marine bivalves. *Environ. Sci. Technol.* **2000**, *34*, 4571−4576.
(17) Santschi, P. H. Marine colloids, agents of the self-cleansing capacity of aquatic systems: Historical perspective and new discoveries. *Mar. Chem.* **2018**, *207*, 124−135.
(18) Guo, L.; Santschi, P. H. Composition and cycling of colloids in marine environments. *Rev. Geophys.* **1997**, *35*, 17−40.
(19) Jensen, L. T.; Lanning, N. T.; Marsay, C. M.; Buck, C. S.; Aguilar-Islas, A. M.; Rember, R.; Landing, W. M.; Sherrell, R. M.; Fitzsimmons, J. N. Biogeochemical cycling of colloidal trace metals in the Arctic cryosphere. *J. Geophys. Res.: Oceans* **2021**, *126*, No. e2021JC017394.
(20) Sun, T. R.; Levin, B. D. A.; Schmidt, M. P.; Guzman, J. J. L.; Enders, A.; Martinez, C. E.; Muller, D. A.; Angenent, L. T.; Lehmann, J. Simultaneous quantification of electron transfer by carbon matrices and functional groups in pyrogenic carbon. *Environ. Sci. Technol.* **2018**, *52*, 8538−8547.
(21) Kang, W. L.; Yu, F. B.; Wang, S. T.; Hu, X. G. Marine colloids promote the adaptation of diatoms to nitrate contamination by directional electron transfer. *Environ. Sci. Technol.* **2022**, *56*, 5694−5705.
(22) Huang, S. F.; Chen, M.; Diao, Y. M.; Feng, Q. Y.; Zeng, R. J.; Zhou, S. G. Dissolved organic matter acting as a microbial photosensitizer drives photoelectrotrophic denitrification. *Environ. Sci. Technol.* **2022**, *56*, 4632−4641.
(23) Brown, K. A.; Harris, D. F.; Wilker, M. B.; Rasmussen, A.; Khadka, N.; Hamby, H.; Keable, S.; Dukovic, G.; Peters, J. W.; Seefeldt, L. C.; King, P. W. Light-driven dinitrogen reduction catalyzed by a CdS:nitrogenase MoFe protein biohybrid. *Science* **2016**, *352*, 448−450.
(24) Guzman, M. S.; Rengasamy, K.; Binkley, M. M.; Jones, C.; Ranaivoarisoa, T. O.; Singh, R.; Fike, D. A.; Meacham, J. M.; Bose, A. Phototrophic extracellular electron uptake is linked to carbon dioxide fixation in the bacterium *Rhodopseudomonas palustris*. *Nat. Commun.* **2019**, *10*, No. 1355.
(25) Wang, B.; Xiao, K. M.; Jiang, Z. F.; Wang, J. F.; Yu, J. C.; Wong, P. K. Biohybrid photoheterotrophic metabolism for significant enhancement of biological nitrogen fixation in pure microbial cultures. *Energy Environ. Sci.* **2019**, *12*, 2185−2191.
(26) Kang, W. L.; Li, X. K.; Mu, L.; Hu, X. G. Nanoscale colloids induce metabolic disturbance of zebrafish at environmentally relevant concentrations. *Environ. Sci. Nano* **2019**, *6*, 1562−1575.
(27) Prufert-Bebout, L.; Paerl, H. W.; Lassen, C. Growth, nitrogen fixation, and spectral attenuation in cultivated *Trichodesmium* species. *Appl. Environ. Microbiol.* **1993**, *59*, 1367−1375.
(28) Chen, Y.-B.; Zehr, J. P.; Mellon, M. Growth and nitrogen fixation of the diazotrophic filamentous nonheterocystous cyanobacterium *Trichodesmium* sp. IMS 101 in defined media: Evidence for a circadian rhythm. *J. Phycol.* **1996**, *32*, 916−923.
(29) Hong, H.; Shen, R.; Zhang, F.; Wen, Z.; Chang, S.; Lin, W.; Kranz, S. A.; Luo, Y.-W.; Kao, S.-J.; Morel, F. M. M.; Shi, D. The complex effects of ocean acidification on the prominent N_2-fixing cyanobacterium *Trichodesmium*. *Science* **2017**, *356*, 527−531.
(30) Genty, B.; Briantais, J.-M.; Baker, N. R. The relationship between the quantum yield of photosynthetic electron transport and quenching of chlorophyll fluorescence. *Biochim. Biophys. Acta, Gen. Subj.* **1989**, *990*, 87−92.
(31) Chappell, P. D.; Webb, E. A. A molecular assessment of the iron stress response in the two phylogenetic clades of *Trichodesmium*. *Environ. Microbiol.* **2010**, *12*, 13−27.
(32) Breitbarth, E.; Mills, M. M.; Friedrichs, G.; LaRoche, J. The Bunsen gas solubility coefficient of ethylene as a function of temperature and salinity and its importance for nitrogen fixation assays. *Limnol. Oceanogr.: Methods* **2004**, *2*, 282−288.
(33) Nguyen, T. D. K.; Mellander, L.; Lork, A.; Thomen, A.; Philipsen, M.; Kurczy, M. E.; Phan, N. T. N.; Ewing, A. G. Visualization of partial exocytotic content release and chemical transport into nanovesicles in cells. *ACS Nano* **2022**, *16*, 4831−4842.
(34) Raina, J. B.; Clode, P. L.; Cheong, S.; Bougoure, J.; Kilburn, M. R.; Reeder, A.; Foret, S.; Stat, M.; Beltran, V.; Thomas-Hall, P.; Topiolas, D.; Motti, C. M.; Gong, B.; Pernice, M.; Marjo, C. E.; Seymour, J. R.; Willis, B. L.; Bourne, D. G. Subcellular tracking reveals the location of dimethylsulfoniopropionate in microalgae and visualises its uptake by marine bacteria. *eLife* **2017**, *6*, No. e23008.
(35) Zeng, H.; Hu, X. G.; Zhou, Q. X.; Luo, J. W.; Hou, X. Extracellular polymeric substances mediate defect generation and phytotoxicity of single-layer MoS_2. *J. Hazard Mater.* **2022**, *429*, No. 128361.

https://doi.org/10.1021/acs.est.4c01849
Environ. Sci. Technol. 2024, 58, 9236−9249

(36) Vasil'ev, I. R.; Matorin, D. N.; Lyadsky, V. V.; Venediktov, P. S. Multiple action sites for photosystem II herbicides as revealed by delayed fluorescence. *Photosynth. Res.* **1988**, *15*, 33−39.
(37) Pence, N.; Tokmina-Lukaszewska, M.; Yang, Z. Y.; Ledbetter, R. N.; Seefeldt, L. C.; Bothner, B.; Peters, J. W. Unraveling the interactions of the physiological reductant flavodoxin with the different conformations of the Fe protein in the nitrogenase cycle. *J. Biol. Chem.* **2017**, *292*, 15661−15669.
(38) Yang, Z. Y.; Ledbetter, R.; Shaw, S.; Pence, N.; Tokmina-Lukaszewska, M.; Eilers, B.; Guo, Q.; Pokhrel, N.; Cash, V. L.; Dean, D. R.; Antony, E.; Bothner, B.; Peters, J. W.; Seefeldt, L. C. Evidence that the Pi release event is the rate-limiting step in the nitrogenase catalytic cycle. *Biochemistry* **2016**, *55*, 3625−3635.
(39) Chen, M.; Dei, R. C. H.; Wang, W. X.; Guo, L. D. Marine diatom uptake of iron bound with natural colloids of different origins. *Mar. Chem.* **2003**, *81*, 177−189.
(40) Yin, Y. G.; Liu, J. F.; Jiang, G. B. Sunlight-induced reduction of ionic Ag and Au to metallic nanoparticles by dissolved organic matter. *ACS Nano* **2012**, *6*, 7910−7919.
(41) Sharma, V. K.; Filip, J.; Zboril, R.; Varma, R. S. Natural inorganic nanoparticles - formation, fate, and toxicity in the environment. *Chem. Soc. Rev.* **2015**, *44*, 8410−8423.
(42) Hochella, M. F.; Mogk, D. W.; Ranville, J.; Allen, I. C.; Luther, G. W.; Marr, L. C.; McGrail, B. P.; Murayama, M.; Qafoku, N. P.; Rosso, K. M.; Sahai, N.; Schroeder, P. A.; Vikesland, P.; Westerhoff, P.; Yang, Y. Natural, incidental, and engineered nanomaterials and their impacts on the Earth system. *Science* **2019**, *363*, No. eaau8299.
(43) Zhang, Q.; Wang, R. Y.; Feng, B. W.; Zhong, X. X.; Ostrikov, K. Photoluminescence mechanism of carbon dots: triggering high-color-purity red fluorescence emission through edge amino protonation. *Nat. Commun.* **2021**, *12*, No. 6856.
(44) Li, H. Y.; Xu, Y.; Ding, J.; Zhao, L.; Zhou, T. Y.; Ding, H.; Chen, Y. H.; Ding, L. Microwave-assisted synthesis of highly luminescent N- and S-co-doped carbon dots as a ratiometric fluorescent probe for levofloxacin. *Microchim. Acta* **2018**, *185*, No. 104, DOI: 10.1007/s00604-017-2619-z.
(45) Walpen, N.; Schroth, M. H.; Sander, M. Quantification of phenolic antioxidant moieties in dissolved organic matter by flow-injection analysis with electrochemical detection. *Environ. Sci. Technol.* **2016**, *50*, 6423−6432.
(46) Chen, X. Y.; Feng, Q. Y.; Cai, Q. H.; Huang, S. F.; Yu, Y. Q.; Zeng, R. J.; Chen, M.; Zhou, S. G. Mn_3O_4 nanozyme coating accelerates nitrate reduction and decreases N_2O emission during photoelectrotrophic denitrification by *Thiobacillus denitrificans*-CdS. *Environ. Sci. Technol.* **2020**, *54*, 10820−10830.
(47) Huang, S. F.; Chen, K. Y.; Chen, X. Y.; Liao, H. P.; Zeng, R. J.; Zhou, S. G.; Chen, M. Sunlight significantly enhances soil denitrification via an interfacial biophotoelectrochemical pathway. *Environ. Sci. Technol.* **2023**, *57*, 7733−7742.
(48) Parola, S.; Julián-López, B.; Carlos, L. D.; Sanchez, C. Optical properties of hybrid organic-inorganic materials and their applications. *Adv. Funct. Mater.* **2016**, *26*, 6506−6544.
(49) Liang, Z.; Letscher, R. T.; Knapp, A. N. Global patterns of surface ocean dissolved organic matter stoichiometry. *Global Biogeochem. Cycles* **2023**, *37*, No. e2023GB007788, DOI: 10.1029/2023GB007788.
(50) Benavides, M.; Berthelot, H.; Duhamel, S.; Raimbault, P.; Bonnet, S. Dissolved organic matter uptake by Trichodesmium in the Southwest Pacific. *Sci. Rep.* **2017**, *7*, No. 41315.
(51) Lu, A. H.; Li, Y.; Ding, H. R.; Xu, X. M.; Li, Y. Z.; Ren, G. P.; Liang, J.; Liu, Y. W.; Hong, H.; Chen, N.; Chu, S. Q.; Liu, F. F.; Li, Y.; Wang, H. R.; Ding, C.; Wang, C. Q.; Lai, Y.; Liu, J.; Dick, J.; Liu, K. H.; Hochella, M. F. Photoelectric conversion on Earth's surface via widespread Fe- and Mn-mineral coatings. *Proc. Natl. Acad. Sci. U.S.A.* **2019**, *116*, 9741−9746, DOI: 10.1073/pnas.1902473116.
(52) Zheng, Y.; Wang, H.; Liu, Y.; Liu, P.; Zhu, B.; Zheng, Y.; Li, J.; Chistoserdova, L.; Ren, Z. J.; Zhao, F. Electrochemically coupled CH_4 and CO_2 consumption driven by microbial processes. *Nat. Commun.* **2024**, *15*, No. 3097.
(53) Pietsch, D.; Bernat, G.; Kahmann, U.; Staiger, D.; Pistorius, E. K.; Michel, K. P. New insights into the function of the iron deficiency-induced protein C from *Synechococcus elongatus* PCC 7942. *Photosynth. Res.* **2011**, *108*, 121−132.
(54) Hill, N. C.; Tay, J. W.; Altus, S.; Bortz, D. M.; Cameron, J. C. Life cycle of a cyanobacterial carboxysome. *Sci. Adv.* **2020**, *6*, No. eaba1269.
(55) Zhang, F. T.; Wen, Z. Z.; Wang, S. L.; Tang, W. Y.; Luo, Y. W.; Kranz, S. A.; Hong, H. Z.; Shi, D. L. Phosphate limitation intensifies negative effects of ocean acidification on globally important nitrogen fixing cyanobacterium. *Nat. Commun.* **2022**, *13*, No. 6730.
(56) Muro-Pastor, M. I.; Reyes, J. C.; Florencio, F. J. Ammonium assimilation in cyanobacteria. *Photosynth. Res.* **2005**, *83*, 135−150.
(57) Zhang, C. C.; Zhou, C. Z.; Burnap, R. L.; Peng, L. Carbon/nitrogen metabolic balance: Lessons from cyanobacteria. *Trends Plant Sci.* **2018**, *23*, 1116−1130.
(58) Robles-Rengel, R.; Florencio, F. J.; Muro-Pastor, M. I. Redox interference in nitrogen status via oxidative stress is mediated by 2-oxoglutarate in cyanobacteria. *New Phytol.* **2019**, *224*, 216−228.
(59) Sekine, R.; Moore, K. L.; Matzke, M.; Vallotton, P.; Jiang, H. B.; Hughes, G. M.; Kirby, J. K.; Donner, E.; Grovenor, C. R. M.; Svendsen, C.; Lombi, E. Complementary imaging of silver nanoparticle interactions with green algae: Dark-field microscopy, electron microscopy, and nanoscale secondary ion mass spectrometry. *ACS Nano* **2017**, *11*, 10894−10902.
(60) Weng, N. Y.; Guagliardo, P.; Jiang, H. B.; Wang, W. X. NanoSIMS imaging of bioaccumulation and subcellular distribution of manganese during oyster gametogenesis. *Environ. Sci. Technol.* **2021**, *55*, 8223−8235.
(61) Ran, M.; Du, B.; Liu, W.; Liang, Z.; Liang, L.; Zhang, Y.; Zeng, L.; Xing, M. Dynamic defects boost in-situ H_2O_2 piezocatalysis for water cleanup. *Proc. Natl. Acad. Sci. U.S.A.* **2024**, *121*, No. e2317435121.
(62) Zhu, X. Y.; Xu, Z. J.; Tang, H. T.; Nie, L. H.; Nie, R.; Wang, R. F.; Liu, X. M.; Huang, X. Photosynthesis-mediated intracellular biomineralization of gold nanoparticles inside cells towards hydrogen boosting under green light. *Angew. Chem., Int. Ed.* **2023**, *62*, No. e202308437, DOI: 10.1002/anie.202308437.
(63) Dong, F. Y.; Lee, Y. S.; Gaffney, E. M.; Liou, W.; Minteer, S. D. Engineering cyanobacterium with transmembrane electron transfer ability for bioelectrochemical nitrogen fixation. *ACS Catal.* **2021**, *11*, 13169−13179.
(64) Yu, L. P.; Yuan, Y.; Rensing, C.; Zhou, S. G. Combined spectroelectrochemical and proteomic characterizations of bidirectional *Alcaligenes faecalis*-electrode electron transfer. *Biosens. Bioelectron.* **2018**, *106*, 21−28.
(65) Battchikova, N.; Aro, E. M. Cyanobacterial NDH-1 complexes: Multiplicity in function and subunit composition. *Physiol. Plant.* **2007**, *131*, 22−32.
(66) Koh, S.; Choi, Y.; Lee, I.; Kim, G. M.; Kim, J.; Park, Y. S.; Lee, S. Y.; Lee, D. C. Light-driven ammonia production by *Azotobacter vinelandii* cultured in medium containing colloidal quantum dots. *J. Am. Chem. Soc.* **2022**, *144*, 10798−10808.
(67) Cerdan-Garcia, E.; Baylay, A.; Polyviou, D.; Woodward, E. M. S.; Wrightson, L.; Mahaffey, C.; Lohan, M. C.; Moore, C. M.; Bibby, T. S.; Robidart, J. C. Transcriptional responses of Trichodesmium to natural inverse gradients of Fe and P availability. *ISME J.* **2022**, *16*, 1055−1064.
(68) Finzi-Hart, J. A.; Pett-Ridge, J.; Weber, P. K.; Popa, R.; Fallon, S. J.; Gunderson, T.; Hutcheon, I. D.; Nealson, K. H.; Capone, D. G. Fixation and fate of C and N in the cyanobacterium *Trichodesmium* using nanometer-scale secondary ion mass spectrometry. *Proc. Natl. Acad. Sci. U.S.A.* **2009**, *106*, 9931.
(69) Zehr, J. P.; Capone, D. G. Changing perspectives in marine nitrogen fixation. *Science* **2020**, *368*, No. eaay9514.
(70) Fowler, D.; Pyle, J. A.; Raven, J. A.; Sutton, M. A. The global nitrogen cycle in the twenty-first century: Introduction. *Philos. Trans. R. Soc., B* **2013**, *368*, No. 20130165.

(71) Berman-Frank, I.; Lundgren, P.; Chen, Y. B.; Küpper, H.; Kolber, Z.; Bergman, B.; Falkowski, P. Segregation of nitrogen fixation and oxygenic photosynthesis in the marine cyanobacterium. *Science* **2001**, *294*, 1534−1537.
(72) Luo, W.; Inomura, K.; Zhang, H.; Luo, Y. W. N_2 fixation in *Trichodesmium* does not require spatial segregation from photosynthesis. *mSystems* **2022**, *7*, No. e0053822.

https://doi.org/10.1021/acs.est.4c01849
Environ. Sci. Technol. 2024, 58, 9236−9249